JOURNAL OF PROPULSION AND POWER
Vol. 9, No. 2, March–April 1993

Quasi-Three-Dimensional Nonreflecting Boundary Conditions for Euler Equations Calculations

André P. Saxer* and Michael B. Giles†
Massachusetts Institute of Technology, Cambridge, Massachusetts 02139

This article presents a theory for the construction of steady-state quasi-three-dimensional nonreflecting boundary conditions for the Euler equations. These allow calculations to be performed on truncated domains without the generation of spurious nonphysical reflections at the far-field boundaries. The theory is based upon Fourier analysis and eigenvectors applied to the linearized Euler equations. It is presented within the context of transonic axial flow turbomachinery computations. The effectiveness of the new boundary conditions is demonstrated by comparing results obtained using this new formulation and calculations performed with the standard one-dimensional approach.

Nomenclature

c	=	speed of sound
h_t	=	stagnation enthalpy
k, l	=	wave numbers in the x and y directions, respectively
P	=	pitch
p	=	static pressure
p_t	=	stagnation pressure
R	=	radius, $\sqrt{y^2 + z^2}$
s	=	entropy
t	=	time
U	=	vector of primitive variables
u, v, w	=	Cartesian velocity components in x, y, z directions, respectively
u_x, u_θ, u_R	=	cylindrical velocity components in x, θ, R directions, respectively
u^R, v^L	=	right and left eigenvectors
α_θ, α_R	=	tangential and radial flow angles, respectively
β	=	pressure wave parameter
γ	=	ratio of specific heats
ρ	=	static density
σ	=	under-relaxation factor
Φ	=	vector of linearized characteristic variables
Ω	=	angular speed

Subscripts

F	=	flux-averaged quantity
inl	=	inlet
out	=	outlet

Superscripts

n	=	time index
$\bar{}$	=	circumferential arithmetic average
$\hat{}$	=	Fourier transformed quantity
$\tilde{}$	=	linearized perturbation

Presented as Paper 91-1603 at the AIAA 10th Computational Fluid Dynamics Conference, Honolulu, HI, June 24–26, 1991; received February 27, 1992; revision received May 30, 1992; accepted for publication June 9, 1992. Copyright © 1992 by the American Institute of Aeronautics and Astronautics, Inc. All rights reserved.

*Research Associate, Computational Fluid Dynamics Laboratory, Department of Aeronautics and Astronautics; currently at Institute of Energy Technology, ETH-Zentrum, 8092 Zürich, Switzerland. Member AIAA.

†Associate Professor, Computational Fluid Dynamics Laboratory, Department of Aeronautics and Astronautics, currently at Oxford University Computing Laboratory, Oxford OX11AA, England, United Kingdom. Member AIAA.

I. Introduction

ONE typical difficulty occurring in a numerical simulation of a turbomachine flowfield is the handling of the boundary conditions (b.c.). This is because in an internal flow environment the computation has to be performed on truncated domains, whose far-field boundaries do not represent an undisturbed known flowfield as in external aerodynamics. Typically, most of the codes available today are not capable of preventing spurious, nonphysical reflections at inflow and outflow boundaries. This leads to erroneous performance predictions, since the calculated flowfield is dependent on the position of the far-field boundary condition. Also for secondary flow calculations accurate boundary conditions are needed since using the standard one-dimensional approach corrupts the solution locally, as shown later in the results section.

The theoretical foundations of nonreflecting boundary conditions for model initial boundary value problems have been established by mathematicians specializing in the analysis of partial differential equations, see for instance Refs. 1 and 2. Some applications involving the Euler equations of fluid dynamics have been done. For two-dimensional steady-state flow, exact nonreflecting boundary conditions for the solution of the linearized Euler equations can be derived using Fourier expansion in the direction along the inlet and the exit boundaries. This has been done by Ferm and Gustafsson for an airfoil and a channel flow.[3,4] Hirsch and Verhoff[5] used a similar approach for cascade flows, though expanding the characteristic variables instead of the primitive ones used by Ferm and Gustafsson. In Ref. 6 Giles presented a unified theory on the formulation of nonreflecting boundary conditions and the application to the Euler equations. In particular, he derived different types of boundary conditions. These include exact one-dimensional and two-dimensional as well as approximate two-dimensional boundary conditions to be used for steady and unsteady flows. A different approach has been proposed by Bayliss and Turkel.[7] They used the asymptotic behavior of the wave equation to derive a boundary condition formulation for external flows.

The purpose of this article is to present a quasi-three-dimensional nonreflecting boundary condition formulation that can be used in a numerical simulation of steady-state inviscid flowfields. The objective in formulating the nonreflecting boundary conditions is to prevent nonphysical reflections at inflow and outflow boundaries as well as at stator/rotor interfaces. The method is an adaptation of the exact two-dimensional steady nonreflecting boundary conditions of Giles[6] to three dimensions. The theoretical approach, based upon Fourier analysis and eigenvectors is presented here, as well

as the extensions required for the linearized Euler equations. Implemented in a turbomachinery environment, the approach assumes that the solution at the boundary is circumferentially decomposed into Fourier modes, the 0^{th} mode corresponding to the average solution. The average mode is treated according to the standard one-dimensional boundary condition formulation which allows the user to specify certain physical quantities at the boundaries. The features of the one-dimensional approach as well as some of its limitations are discussed in Secs. II and III. The remaining part of the solution, represented by the sum of the harmonics, is treated according to the exact two-dimensional theory and prevents spurious reflections at the boundaries. A very brief summary of the theory is that upstream and downstream of the blade row in an infinite duct which produces no incoming modes, the steady-state perturbations in the density, velocity, and pressure must satisfy certain linear relationships. These relationships are found by analyzing the propagation of eigenmodes that are solutions of the linearized Euler equations and vary sinusoidally in the pitchwise direction. Enforcing these relationships at the inflow and outflow boundaries imposes steady-state nonreflecting boundary conditions which ensure that no incoming modes are generated. This approach together with its implementation in a three-dimensional context is discussed in Sec. IV. A brief discussion of the numerical procedure and the stator/rotor interface treatment is presented in Sec. V.

The circumferential Fourier decomposition (vs radial decomposition) is motivated by the fact that in an axial flow turbomachine the pitchwise variations are usually larger than the radial variations. The results presented in Sec. VI show clearly that using this quasi-three-dimensional boundary condition formulation improves the accuracy.

A very brief summary of this article together with the essential conclusions is given in Sec. VII.

II. One-Dimensional Nonreflecting Boundary Conditions

The usual one-dimensional approach is to assume perturbations traveling normal to the boundary in the x direction, see for instance Ref. 8. Hence, the linearized Euler equations written in primitive form reduce to

$$\frac{\partial \boldsymbol{U}}{\partial t} + \bar{A}\frac{\partial \boldsymbol{U}}{\partial x} = 0 \tag{1}$$

where

$$\boldsymbol{U} = \begin{bmatrix} \rho - \bar{\rho} \\ u - \bar{u} \\ v - \bar{v} \\ w - \bar{w} \\ p - \bar{p} \end{bmatrix} = \begin{bmatrix} \tilde{\rho} \\ \tilde{u} \\ \tilde{v} \\ \tilde{w} \\ \tilde{p} \end{bmatrix}, \quad \bar{A} = \begin{bmatrix} \bar{u} & \bar{\rho} & 0 & 0 & 0 \\ 0 & \bar{u} & 0 & 0 & 1/\bar{\rho} \\ 0 & 0 & \bar{u} & 0 & 0 \\ 0 & 0 & 0 & \bar{u} & 0 \\ 0 & \gamma\bar{p} & 0 & 0 & \bar{u} \end{bmatrix} \tag{2}$$

The elements of the vector $\boldsymbol{U}$ represent perturbations from a uniform flow, and the Jacobian matrix $\bar{A}$ is evaluated using those same uniform flow conditions. Notice that this represents only a local linearization of the flow, i.e., within one mesh cell, since when concerned with turbomachinery applications, the coefficients of $\bar{A}$ may still vary with radius for instance.

$\bar{A}$ can be diagonalized by the similarity transformation

$$T^{-1}\bar{A}T = \begin{bmatrix} \bar{u} & 0 & 0 & 0 & 0 \\ 0 & \bar{u} & 0 & 0 & 0 \\ 0 & 0 & \bar{u} & 0 & 0 \\ 0 & 0 & 0 & \bar{u} + \bar{c} & 0 \\ 0 & 0 & 0 & 0 & \bar{u} - \bar{c} \end{bmatrix} = \Lambda \tag{3}$$

where $\bar{c} = \sqrt{\gamma\bar{p}/\bar{\rho}}$ is the mean flow speed of sound. The diagonal components of Λ represent the speed of propagation of five characteristic waves, called the entropy, the two vorticity, and for subsonic flow, the upstream and the downstream irrotational pressure waves, respectively. Multiplication of Eq. (1) by T^{-1} yields

$$\frac{\partial \boldsymbol{\Phi}}{\partial t} + \Lambda\frac{\partial \boldsymbol{\Phi}}{\partial x} = 0 \tag{4}$$

where $\boldsymbol{\Phi} = T^{-1}\boldsymbol{U}$. $\boldsymbol{\Phi}$ is referred to as the vector of linearized characteristic variables, and in detail the five variables are

$$\begin{bmatrix} \phi_1 \\ \phi_2 \\ \phi_3 \\ \phi_4 \\ \phi_5 \end{bmatrix} = \begin{bmatrix} -\bar{c}^2 & 0 & 0 & 0 & 1 \\ 0 & 0 & \bar{\rho}\bar{c} & 0 & 0 \\ 0 & 0 & 0 & \bar{\rho}\bar{c} & 0 \\ 0 & \bar{\rho}\bar{c} & 0 & 0 & 1 \\ 0 & -\bar{\rho}\bar{c} & 0 & 0 & 1 \end{bmatrix} \begin{bmatrix} \tilde{\rho} \\ \tilde{u} \\ \tilde{v} \\ \tilde{w} \\ \tilde{p} \end{bmatrix} \tag{5}$$

The transformation from the one-dimensional characteristic variables is given by $\boldsymbol{U} = T\boldsymbol{\Phi}$, i.e.

$$\begin{bmatrix} \tilde{\rho} \\ \tilde{u} \\ \tilde{v} \\ \tilde{w} \\ \tilde{p} \end{bmatrix} = \begin{bmatrix} -1/\bar{c}^2 & 0 & 0 & 1/(2\bar{c}^2) & 1/(2\bar{c}^2) \\ 0 & 0 & 0 & 1/(2\bar{\rho}\bar{c}) & -1/(2\bar{\rho}\bar{c}) \\ 0 & 1/\bar{\rho}\bar{c} & 0 & 0 & 0 \\ 0 & 0 & 1/\bar{\rho}\bar{c} & 0 & 0 \\ 0 & 0 & 0 & \frac{1}{2} & \frac{1}{2} \end{bmatrix} \begin{bmatrix} \phi_1 \\ \phi_2 \\ \phi_3 \\ \phi_4 \\ \phi_5 \end{bmatrix} \tag{6}$$

At a subsonic inlet the correct unsteady, nonreflecting boundary conditions would be

$$\begin{pmatrix} \phi_1 \\ \phi_2 \\ \phi_3 \\ \phi_4 \end{pmatrix} = 0 \tag{7}$$

while at an outlet the correct nonreflecting boundary condition would be

$$\phi_5 = 0 \tag{8}$$

The standard numerical method for implementing these would be to calculate or extrapolate the outgoing characteristic values from the interior domain, and then use Eq. (6) to reconstruct the solution on the boundary.

III. One-Dimensional Steady-State Reflecting Boundary Conditions

For calculations of steady-state external flows, these one-dimensional boundary conditions may be applied without modification. In these types of calculations the far-field represents uniform conditions in which the inlet flow corresponds to the outlet one. That is, the steady-state perturbations in the density, velocity, and pressure are zero. Hence, setting the incoming characteristics to zero is consistent with uniform flow conditions, so that this boundary condition formulation is nonreflecting.

For time-marching calculations of steady-state internal flows, however, the one-dimensional (unsteady) nonreflecting boundary conditions require modification. In a typical turbomachinery application one wishes to specify certain physical quantities at the boundaries. For example, at the outflow boundary one usually specifies the static pressure. This means that the incoming characteristic variable ϕ_5, instead of being zero, must have the value required to give the correct exit pressure. This is now a reflective boundary condition, since an outgoing unsteady pressure wave will produce an incoming pressure wave to keep the exit pressure constant. Similar unsteady reflections are generated at the inflow boundary through the specification of particular physical quantities such as the stagnation pressure and flow angles.

The numerical implementation of the boundary conditions is dependent on the numerical algorithm being used for the interior equations. Using a Lax-Wendroff type algorithm to time-march the solution to the steady state, the changes in the boundary values from time level n to time level $n + 1$ are required. Thus, the characteristic variables are defined in terms of perturbations to the average inflow or outflow at the time level n.

At the inflow, the average characteristic changes are calculated from the requirement that the average entropy, radial, and tangential flow angles, and stagnation enthalpy have certain values

$$\begin{aligned}(\bar{s})^{n+1} &= \bar{s}_{\text{inl}} \\ (\bar{\alpha}_\theta)^{n+1} &= \alpha_{\theta\,\text{inl}} \\ (\bar{\alpha}_R)^{n+1} &= \alpha_{R\,\text{inl}} \\ (\bar{h}_t)^{n+1} &= \bar{h}_{t\text{inl}}\end{aligned} \tag{9}$$

$\bar{s}$ is an entropy-related function defined by

$$\bar{s} = \overline{\log(\gamma p) - \gamma \log \rho} \tag{10}$$

and $\bar{h}_t$ is the mean total enthalpy. $\alpha_{\theta\,\text{inl}}$ and $\alpha_{R\,\text{inl}}$ together with $\bar{s}_{\text{inl}}$ and $\bar{h}_{t\text{inl}}$ are user-specified average inflow angles, entropy, and total enthalpy, respectively, which are usually a function of the radius.

For an axially subsonic outflow, the first four charateristics are outgoing, so only the fifth characteristic variable needs to be set. The average change in the characteristic is determined to achieve the user-specified average exit pressure $\bar{p}_{\text{out}}$ at a certain radius together with the requirement that the outflow is in radial equilibrium. The latter condition is expressed by

$$\frac{\partial \bar{p}(R)_{\text{out}}}{\partial R} = \bar{\rho}\frac{\bar{u}_\theta^2}{R} \tag{11}$$

together with the specification of $\bar{p}_{\text{out}}$ at some particular radius.

The standard one-dimensional boundary conditions are also "reflective" in a steady-state sense. This is most clearly understood at the outflow boundary where a circumferentially uniform exit pressure has been specified. If the outflow is supersonic there will be an oblique shock extending from the trailing edge to the outflow boundary. The uniform pressure condition forces the generation of a reflected expansion wave at the boundary. This expansion wave extends upstream to the blade row, and can produce significant errors. The objective of the new boundary conditions presented in the next section is to prevent this reflection, and similar reflections at the inflow boundary.

IV. Quasi-Three-Dimensional Approach

A. Outline

By the principle of linear superposition it is possible to split a general solution into a sum of different frequencies and calculate their contributions independently, each with its own forcing terms and boundary conditions. Here we are concerned with axial turbomachines in which the flow variations are usually larger in the circumferential than in the radial direction. Therefore, by assuming a periodic solution in the pitchwise direction it is quite natural to perform a Fourier decomposition of the flow at the boundary into a sum of mean and circumferential components.

In this approach, the 0^{th} Fourier mode corresponds to the circumferential solution average and is treated according to the standard one-dimensional characteristics theory. Specifically, this allows the user to specify the value of the circumferential average characteristics, but these quantities may be radius dependent. For instance, this is how the average inlet tangential, radial flow angles, stagnation enthalpy and entropy can be specified, as well as the outlet radial equilibrium condition.

The remaining part of the solution, represented by the sum of the harmonics, is treated according to Giles' two-dimensional nonreflecting boundary conditions theory.[6] Implemented in three dimensions, this part of the formulation uncouples the tangential flow variation from the radial variation. However, the advantage of this improved approach over the standard one-dimensional formulation is that when sweeping along the span, exact two-dimensional nonreflecting boundary conditions can be imposed on each Fourier mode in the tangential direction.

Since this method considers radial flow variations in the average mode only, it is called "quasi-three-dimensional nonreflecting boundary conditions." Note that in the absence of any radial variations, the boundary conditions are exact within the two-dimensional linear theory.

B. Fourier Analysis: Dispersion Relation

The boundary condition treatment is approached by assuming that the flow is governed by the three-dimensional linearized Euler equations, which, written in primitive form for two-dimensional steady-state variations are

$$\bar{A}\frac{\partial \boldsymbol{U}}{\partial x} + \bar{B}\frac{\partial \boldsymbol{U}}{\partial y} = 0 \tag{12}$$

where $\boldsymbol{U}$ and $\bar{A}$ are given by Eqs. (2) and $\bar{B}$ represents the following matrix:

$$\bar{B} = \begin{bmatrix} \bar{v} & 0 & \bar{\rho} & 0 & 0 \\ 0 & \bar{v} & 0 & 0 & 0 \\ 0 & 0 & \bar{v} & 0 & 1/\bar{\rho} \\ 0 & 0 & 0 & \bar{v} & 0 \\ 0 & 0 & \gamma\bar{p} & 0 & \bar{v} \end{bmatrix} \tag{13}$$

According to the Fourier analysis performed by Giles,[6] wave-like solutions which are equal to a scalar wave function multiplying a constant column vector are considered:

$$\boldsymbol{U}(x, y) = \exp[i(kx + ly)]\boldsymbol{u}^{\text{R}} \tag{14}$$

Substituting this into the differential equation gives

$$(k\bar{A} + l\bar{B})\boldsymbol{u}^{\text{R}} = 0 \tag{15}$$

which has nontrivial solutions provided that

$$\det(k\bar{A} + l\bar{B}) = 0 \tag{16}$$

Evaluating Eq. (16) gives the dispersion relation, which is a polynomial equation of degree 5 in each of k and l.

$$(\bar{u}k + \bar{v}l)^3[(\bar{u}k + \bar{v}l)^2 - \bar{c}^2(k^2 + l^2)] = 0 \tag{17}$$

We will be concerned with the roots k_n of this equation for given values of l.

Three of the five roots are clearly identical:

$$k_{1,2,3} = (-\bar{v}l/\bar{u}) \tag{18}$$

The other two roots are given by

$$(\bar{c}^2 - \bar{u}^2)k^2 - 2\bar{u}\bar{v}kl - (\bar{v}l)^2 + (\bar{c}l)^2 = 0 \tag{19}$$

Hence the fourth and the fifth roots are defined by

$$k_4 = [(\bar{u}\bar{v}l + \bar{c}\beta l)/(\bar{c}^2 - \bar{u}^2)] \tag{20}$$

$$k_5 = [(\bar{u}\bar{v}l - \bar{c}\beta l)/(\bar{c}^2 - \bar{u}^2)] \tag{21}$$

where

$$\beta = \begin{cases} i\,\mathrm{sign}(l)\sqrt{\bar{c}^2 - (\bar{u}^2 + \bar{v}^2)}, & (\bar{u}^2 + \bar{v}^2) < \bar{c}^2 \\ -\mathrm{sign}(\bar{v})\sqrt{(\bar{u}^2 + \bar{v}^2) - \bar{c}^2}, & (\bar{u}^2 + \bar{v}^2) > \bar{c}^2 \end{cases} \quad (22)$$

Notice that for supersonic flow, β does not depend on l. The two relations for β reflect the difference in the behavior of a perturbation propagating in subsonic or supersonic flow. In subsonic flow, the perturbation decays exponentially, whereas in supersonic flow it propagates indefinitely. The appearance of two values of β is further discussed in Ref. 9.

C. Fourier Analysis: Eigenvectors

A critical step in the construction and analysis of boundary conditions is to separate the waves into incoming and outgoing modes. This is accomplished by looking at the velocity of energy propagation, i.e., the group velocity[10] of the five dispersive propagating waves. This would require the introduction of the time-dependent term in Eq. (12), but the direction of propagation is already known from the analysis given in Sec. II.

The column vector $\boldsymbol{u}^R$ is the right null-vector of the singular matrix $(kI + l\bar{A}^{-1}\bar{B})$

$$(kI + \bar{A}^{-1}l\bar{B})\boldsymbol{u}^R = \bar{A}^{-1}(k\bar{A} + l\bar{B})\boldsymbol{u}^R = 0 \quad (23)$$

$\boldsymbol{u}^R$ is a right eigenvector of $l\bar{A}^{-1}\bar{B}$ with eigenvalue $-k$. The construction of the nonreflecting boundary conditions requires also the row vector $\boldsymbol{v}^L$ which is the left null-vector of the singular matrix $\bar{A}^{-1}(k\bar{A} + l\bar{B})$:

$$\boldsymbol{v}^L\bar{A}^{-1}(k\bar{A} + l\bar{B}) = 0 \quad (24)$$

The important feature of this left null-vector is its orthogonality to $\boldsymbol{u}^R$. If k_m and k_n are two different solutions of the dispersion relation for the same values of l, and if $\boldsymbol{u}_m^R$ and $\boldsymbol{v}_n^L$ are the corresponding right and left eigenvectors, then

$$\boldsymbol{v}_n^L\bar{A}^{-1}(k_m\bar{A} + l\bar{B})\boldsymbol{u}_m^R = 0 \quad (25)$$

$$\boldsymbol{v}_n^L\bar{A}^{-1}(k_n\bar{A} + l\bar{B})\boldsymbol{u}_m^R = 0 \quad (26)$$

Subtracting one from the other gives

$$(k_m - k_n)\boldsymbol{v}_n^L\boldsymbol{u}_m^R = 0 \Rightarrow \boldsymbol{v}_n^L\boldsymbol{u}_m^R = 0 \quad (27)$$

This orthogonality condition will be used later in the next section.

Root 1: Entropy Wave

$$k_1 = (-\bar{v}l/\bar{u}) \quad (28)$$

After some algebra, it can be shown that appropriate right and left orthonormal eigenvectors are

$$\boldsymbol{u}_1^R = \begin{bmatrix} -1/\bar{c}^2 \\ 0 \\ 0 \\ 0 \\ 0 \end{bmatrix} \quad (29)$$

$$\boldsymbol{v}_1^L = (-\bar{c}^2 \quad 0 \quad 0 \quad 0 \quad 1) \quad (30)$$

This choice of eigenvectors corresponds to the entropy wave. This can be verified by noting that the only nonzero term in the right eigenvector is the density, so that the wave has varying entropy, no vorticity, and constant pressure. Also, the left eigenvector "measures" entropy in the sense that $\boldsymbol{v}_1^L U$ is equal to the linearized entropy, $\bar{p} - \bar{c}^1\bar{\rho}$.

Root 2: First Vorticity Wave

$$k_2 = (-\bar{v}l/\bar{u}) \quad (31)$$

The second set of right and left eigenvectors for the multiple root is given by

$$\boldsymbol{u}_2^R = (1/\bar{\rho}\bar{c})\begin{bmatrix} 0 \\ -l^2/\bar{u}k_2^2 \\ l/\bar{u}k_2 \\ 0 \\ 0 \end{bmatrix} = (1/\bar{\rho}\bar{c})\begin{bmatrix} 0 \\ -\bar{u}/\bar{v}^2 \\ -1/\bar{v} \\ 0 \\ 0 \end{bmatrix} \quad (32)$$

$$\boldsymbol{v}_2^L = \bar{\rho}\bar{c}(0 \quad -\bar{u} \quad -\bar{v} \quad 0 \quad -1/\bar{\rho}) \quad (33)$$

This root corresponds to a vorticity wave, which can be verified by noting that the right eigenvector gives a wave with vorticity, but uniform entropy and pressure.

Root 3: Second Vorticity Wave

$$k_3 = (-\bar{v}l/\bar{u}) \quad (34)$$

The third set of right and left eigenvectors for the multiple root is given by

$$\boldsymbol{u}_3^R = (1/\bar{\rho}\bar{c})\begin{bmatrix} 0 \\ 0 \\ 0 \\ l/\bar{u}k_3 \\ 0 \end{bmatrix} = (1/\bar{\rho}\bar{c})\begin{bmatrix} 0 \\ 0 \\ 0 \\ -1/\bar{v} \\ 0 \end{bmatrix} \quad (35)$$

$$\boldsymbol{v}_3^L = \bar{\rho}\bar{c}(0 \quad 0 \quad 0 \quad -\bar{v} \quad 0) \quad (36)$$

As with root 2, this set of eigenvectors corresponds to a vorticity wave.

Since the first three roots are a multiple root we must check that the chosen right and left eigenvectors satisfy the necessary orthogonality relations:

$$\boldsymbol{v}_n^L\boldsymbol{u}_m^R = 0, \qquad n, m = 1, 2, 3, \qquad n \neq m \quad (37)$$

It is easily verified that these are correct.

Root 4: Downstream-Running Pressure Wave

$$k_4 = [(\bar{u}\bar{v}l + \bar{c}\beta l)/(\bar{c}^2 - \bar{u}^2)] \quad (38)$$

The eigenvectors are

$$\boldsymbol{u}_4^R = [(\bar{c} + \bar{u})/2\bar{\rho}\bar{c}]\begin{bmatrix} (\bar{\rho}/\bar{c}^2)(-\bar{u}k_4/l - \bar{v}) \\ k_4/l \\ 1 \\ 0 \\ \bar{\rho}(-\bar{u}k_4/l - \bar{v}) \end{bmatrix}$$

$$= \{1/[2\bar{\rho}\bar{c}(\bar{c} - \bar{u})]\}\begin{bmatrix} -(\bar{\rho}/\bar{c})(\bar{c}\bar{v} + \bar{u}\beta) \\ \bar{c}\beta + \bar{u}\bar{v} \\ \bar{c}^2 - \bar{u}^2 \\ 0 \\ -\bar{\rho}\bar{c}(\bar{c}\bar{v} + \bar{u}\beta) \end{bmatrix} \quad (39)$$

$$\boldsymbol{v}_4^L = \bar{\rho}\bar{c}(0 \quad -\bar{v} \quad \bar{u} \quad 0 \quad \beta/\bar{\rho}\bar{c}) \quad (40)$$

This root corresponds to an isentropic, irrotational pressure wave, traveling downstream.

Root 5: Upstream-Running Pressure Wave

$$k_5 = [(\bar{u}\bar{v}l - \bar{c}\beta l)/(\bar{c}^2 - \bar{u}^2)] \quad (41)$$

The eigenvectors are

$$\boldsymbol{u}_5^R = [(\bar{c} - \bar{u})/2\bar{\rho}\bar{c}] \begin{bmatrix} (\bar{\rho}/\bar{c}^2)(-\bar{u}k_5/l - \bar{v}) \\ k_5/l \\ 1 \\ 0 \\ \bar{\rho}(-\bar{u}k_5/l - \bar{v}) \end{bmatrix}$$

$$= \{1/[2\bar{\rho}\bar{c}(\bar{c} + \bar{u})]\} \begin{bmatrix} -(\bar{\rho}/\bar{c})(\bar{c}\bar{v} - \bar{u}\beta) \\ -\bar{c}\beta + \bar{u}\bar{v} \\ \bar{c}^2 - \bar{u}^2 \\ 0 \\ -\bar{\rho}\bar{c}(\bar{c}\bar{v} - \bar{u}\beta) \end{bmatrix} \tag{42}$$

$$\boldsymbol{v}_5^L = \bar{\rho}\bar{c}(0 \quad \bar{v} \quad -\bar{u} \quad 0 \quad \beta/\bar{\rho}\bar{c}) \tag{43}$$

This root corresponds to an isentropic, irrotational pressure wave, traveling upstream provided $\bar{u} < \bar{c}$.

Note that the above defined eigenvectors are only determined to within an arbitrary factor.

D. Ideal Two-Dimensional Steady Nonreflecting Boundary Conditions

Suppose that the differential equation is to be solved in the domain $x > 0$, and one wants to construct nonreflecting boundary conditions at $x = 0$ to minimize or ideally prevent the reflection of outgoing waves. At the boundary at $x = 0$, $\boldsymbol{U}$ can be decomposed into a sum of Fourier modes with different values of l, so the analysis begins by considering just one particular choice of l. In this case the most general form for $\boldsymbol{U}$ is

$$\boldsymbol{U}(x, y) = \left(\sum_{n=1}^{5} a_n \boldsymbol{u}_n^R e^{ik_n x} \right) e^{ily} \tag{44}$$

k_n is the n^{th} root of the dispersion relation for the given value of l, and $\boldsymbol{u}_n^R$ is the corresponding right eigenvector.

The ideal nonreflecting boundary conditions would be to specify that $a_n = 0$ for each n that corresponds to an incoming wave. Because of orthogonality

$$\boldsymbol{v}_n^L \boldsymbol{U} = \boldsymbol{v}_n^L \left(\sum_{m=1}^{5} a_m \boldsymbol{u}_m^R e^{ik_m x} \right) e^{ily}$$

$$= a_n (\boldsymbol{v}_n^L \boldsymbol{u}_n^R) e^{ik_n x} e^{ily} \tag{45}$$

and so an equivalent specification of nonreflecting boundary conditions is

$$\boldsymbol{v}_n^L \boldsymbol{U} = 0 \tag{46}$$

for each n corresponding to an incoming mode, i.e., $n = 1$, 2, 3, 4 at the inflow and $n = 5$ at the outflow.

Both the right $\boldsymbol{u}^R$ and left $\boldsymbol{v}^L$ eigenvectors as defined in Secs. IV.B and IV.C have a physical significance. As used in Eq. (44), the right eigenvector shows the variation in the primitive variables caused by a particular wave mode. Due to the orthogonality relations, the left eigenvector provides a measure of the amplitude of a particular wave component when applied to a general solution.

E. Extension to Three-Dimensions

As mentioned earlier, the construction of the quasi-three-dimensional nonreflecting boundary conditions starts by performing a Fourier decomposition of the flowfield at the boundary. We begin by considering a linear cascade with pitch P in the y direction and a boundary at $x = 0$. The perturbation $\boldsymbol{U}$ can be written as

$$\boldsymbol{U}(0, y, z, t) = \bar{\boldsymbol{U}}(z, t) + \sum_{-\infty, m \neq 0}^{\infty} \hat{\boldsymbol{U}}_m(z, t) e^{ilmy} \tag{47}$$

where $\bar{\boldsymbol{U}}(z, t)$ represents the pitchwise solution average at the boundary that has been constructed according to the standard one-dimensional approach. It also corresponds to the $m = 0$ Fourier mode, whereas the harmonics are defined by

$$\hat{\boldsymbol{U}}_m(z, t) = \frac{1}{P} \int_0^P \boldsymbol{U}(0, y, z, t) e^{-ilmy} \, dy \tag{48}$$

where

$$l_m = (2\pi m/P) \tag{49}$$

At each spanwise location, ideal two-dimensional steady-state nonreflecting boundary conditions can now be constructed for each Fourier mode m, $(m \neq 0)$, according to Sec. IV.D.

The boundary conditions for $(m \neq 0)$ are

$$\boldsymbol{v}_n^L \hat{\boldsymbol{U}}_m = 0 \tag{50}$$

for each incoming wave n. Using the eigenvectors defined in Sec. IV.C the nonreflecting boundary conditions are

$$\begin{pmatrix} -\bar{c}^2 & 0 & 0 & 0 & 1 \\ 0 & -\bar{\rho}\bar{c}\bar{u} & -\bar{\rho}\bar{c}\bar{v} & 0 & -\bar{c} \\ 0 & 0 & 0 & -\bar{\rho}\bar{c}\bar{v} & 0 \\ 0 & -\bar{\rho}\bar{c}\bar{v} & \bar{\rho}\bar{c}\bar{u} & 0 & \beta \end{pmatrix} \hat{\boldsymbol{U}}_m = 0 \tag{51}$$

at the inflow, and at the outflow the boundary condition is

$$(0 \quad \bar{\rho}\bar{c}\bar{v} \quad -\bar{\rho}\bar{c}\bar{u} \quad 0 \quad \beta)\hat{\boldsymbol{U}}_m = 0 \tag{52}$$

The nonreflecting boundary conditions are now expressed in terms of the spatial Fourier transform of the one-dimensional characteristic variables:

$$\hat{\boldsymbol{U}}_m = \begin{bmatrix} -1/\bar{c}^2 & 0 & 0 & 1/(2\bar{c}^2) & 1/(2\bar{c}^2) \\ 0 & 0 & 0 & 1/(2\bar{\rho}\bar{c}) & -1/(2\bar{\rho}\bar{c}) \\ 0 & 1/\bar{\rho}\bar{c} & 0 & 0 & 0 \\ 0 & 0 & 1/\bar{\rho}\bar{c} & 0 & 0 \\ 0 & 0 & 0 & \tfrac{1}{2} & \tfrac{1}{2} \end{bmatrix} \begin{bmatrix} \hat{\phi}_1 \\ \hat{\phi}_2 \\ \hat{\phi}_3 \\ \hat{\phi}_4 \\ \hat{\phi}_5 \end{bmatrix} \tag{53}$$

Therefore, the inflow boundary condition becomes

$$\begin{pmatrix} 1 & 0 & 0 & 0 & 0 \\ 0 & -\bar{v} & 0 & -\tfrac{1}{2}(\bar{c} + \bar{u}) & -\tfrac{1}{2}(\bar{c} - \bar{u}) \\ 0 & 0 & \bar{v} & 0 & 0 \\ 0 & \bar{u} & 0 & \tfrac{1}{2}(\beta - \bar{v}) & \tfrac{1}{2}(\beta + \bar{v}) \end{pmatrix} \begin{bmatrix} \hat{\phi}_1 \\ \hat{\phi}_2 \\ \hat{\phi}_3 \\ \hat{\phi}_4 \\ \hat{\phi}_5 \end{bmatrix} = 0 \tag{54}$$

and the outflow equation becomes

$$(0 \quad -\bar{u} \quad 0 \quad \tfrac{1}{2}(\beta + \bar{v}) \quad \tfrac{1}{2}(\beta - \bar{v})) \begin{bmatrix} \hat{\phi}_1 \\ \hat{\phi}_2 \\ \hat{\phi}_3 \\ \hat{\phi}_4 \\ \hat{\phi}_5 \end{bmatrix} = 0 \tag{55}$$

Unlike the standard one-dimensional approach in which the harmonics of the incoming characteristics are set to zero, this improved method defines the incoming characteristics to be

function of the outgoing ones by using Eqs. (54) and (55). This gives

$$\begin{pmatrix} \hat{\phi}_1 \\ \hat{\phi}_2 \\ \hat{\phi}_3 \\ \hat{\phi}_4 \end{pmatrix} = \begin{bmatrix} 0 \\ -[(\beta + \bar{v})/(\bar{c} + \bar{u})]\hat{\phi}_5 \\ 0 \\ [(\beta + \bar{v})/(\bar{c} + \bar{u})]^2\hat{\phi}_5 \end{bmatrix} \tag{56}$$

$$\hat{\phi}_5 = [2\bar{u}/(\beta - \bar{v})]\hat{\phi}_2 - [(\beta + \bar{v})/(\beta - \bar{v})]\hat{\phi}_4 \tag{57}$$

These algebraic relations are then time-lagged (see Refs. 6 and 9) to ensure the well-posedness of the pseudotime evolution process, so that finally the exact (in a two-dimensional sense), steady b.c. turn out to be

At Inflow

$$\frac{\partial}{\partial t}\begin{pmatrix} \hat{\phi}_1 \\ \hat{\phi}_2 \\ \hat{\phi}_3 \\ \hat{\phi}_4 \end{pmatrix} = \sigma \begin{pmatrix} -\hat{\phi}_1 \\ -[(\beta + \bar{v})/(\bar{c} + \bar{u})]\hat{\phi}_5 - \hat{\phi}_2 \\ -\hat{\phi}_3 \\ [(\beta + \bar{v})/(\bar{c} + \bar{u})]^2\hat{\phi}_5 - \hat{\phi}_4 \end{pmatrix} \tag{58}$$

At Outflow

$$\frac{\partial \hat{\phi}_5}{\partial t} = \sigma\left[\left(\frac{2\bar{u}}{\beta - \bar{v}}\right)\hat{\phi}_2 - \left(\frac{\beta + \bar{v}}{\beta - \bar{v}}\right)\hat{\phi}_4 - \hat{\phi}_5\right] \tag{59}$$

Numerical experience indicates that a suitable choice of σ is $\bar{c}/P$.

Boundary conditions for an annular cascade with many blades are obtained from these linear cascade b.c. by substituting (θ, R) for (y, z) and (u_θ, u_R) for (v, w). This approximation implicitly assumes that the blade pitch is much smaller than the tip radius, which is true for many turbomachine applications. The error associated with this approximation is believed to be smaller than the error arising because of the uncoupled radial and tangential modes.

V. Implementation Procedure and Stator/Rotor Interface Treatment

The procedure to solve the Euler equations on the interior domain uses Ni's[11] version of the Lax-Wendroff algorithm which has been extended to three-dimensions.[12,13] The numerical implementation of the quasi-three-dimensional boundary conditions is briefly outlined here. At the inflow and outflow, the changes in the outgoing characteristics are obtained from the changes distributed by the Lax-Wendroff algorithm. For incoming modes, the average changes in the characteristics are found according to the procedure described in Sec. III, whereas the local changes in the characteristic variables at each point on the inflow and outflow due to the variation in the characteristic variables along the boundary are found as follows. A discrete Fourier transform of the outgoing characteristics is performed which enables the steady-state amplitude of the Fourier transform of the desired incoming characteristics to be calculated according to Eqs. (56) and (57). These are converted back into the physical domain, then compared to the local characteristics and the resulting corrections time-lagged. Now that the local changes in the characteristic variables have been established, these are added to the average changes. The combined five characteristic changes in physical space are then transformed into changes in the primitive variables, and hence, in conservation variables.

Reference 13 describes how the same boundary condition approach can be used to match together a stator and a rotor calculation, so that the interface is treated in a manner that conserves mass, momentum, and energy. In this technique, the average characteristic changes at the stator outflow and the rotor inflow are set to eliminate the following characteristic jumps, taking note of the direction of propagation of each characteristic

$$\begin{bmatrix} \Delta\bar{\phi}_1 \\ \Delta\bar{\phi}_2 \\ \Delta\bar{\phi}_3 \\ \Delta\bar{\phi}_4 \\ \Delta\bar{\phi}_5 \end{bmatrix} = \begin{bmatrix} -\bar{c}^2 & 0 & 0 & 0 & 1 \\ 0 & 0 & \bar{\rho}\bar{c} & 0 & 0 \\ 0 & 0 & 0 & \bar{\rho}\bar{c} & 0 \\ 0 & \bar{\rho}\bar{c} & 0 & 0 & 1 \\ 0 & -\bar{\rho}\bar{c} & 0 & 0 & 1 \end{bmatrix} \begin{bmatrix} \rho_{F\text{stator}} - \rho_{F\text{rotor}} \\ u_{xF\text{stator}} - u_{xF\text{rotor}} \\ u_{\theta F\text{stator}} - u_{\theta F\text{rotor}} - \Omega R \\ u_{RF\text{stator}} - u_{RF\text{rotor}} \\ p_{F\text{stator}} - p_{F\text{rotor}} \end{bmatrix} \tag{60}$$

where ρ_F, u_{xF}, $u_{\theta F}$, u_{RF}, and p_F represent the stream-thrust flux-averaged values of density, axial, circumferential, and radial velocity components and pressure, respectively. Note that because of the use of relative flow variables, the rotor wheel speed ΩR has to be introduced into the condition of matching circumferential velocities. Once this is done for both sides of the interface, the remainder of the boundary condition treatment is exactly the same as for a standard inflow and outflow boundary.

VI. Results

The effectiveness of the steady-state quasi-three-dimensional nonreflecting boundary conditions is demonstrated by presenting results for the high-turning turbine stage represented in Figs. 1 and 2. The design of this stage was performed by Rolls-Royce and is representative of a high pressure, cooled aircraft turbine operating in the transonic regime. In particular, the small axial gap between the stator trailing edge and the rotor leading edge (approximately 30% of the vane axial chord) is typical for this kind of turbine. For these closely spaced blades the formulation of the boundary conditions at the stator/rotor interface becomes a key point in the numerical simulation.

Firstly, results are presented for computations performed on the inlet guide vane alone, i.e., no rotor row attached downstream. The midspan flowfields shown in Fig. 3 have been calculated for supersonic outflow conditions (but still axially subsonic), with two different locations of the far-field boundaries. Notice that the location of the small domain exit boundary corresponds to the stator/rotor interface position in the computations of the complete state reported later in this section. The solutions look very similar, although not identical due to the second-order nonlinear effects caused by the presence of two weak oblique shocks extending from the trailing edge. Indeed, the linearization of the Euler equations at the

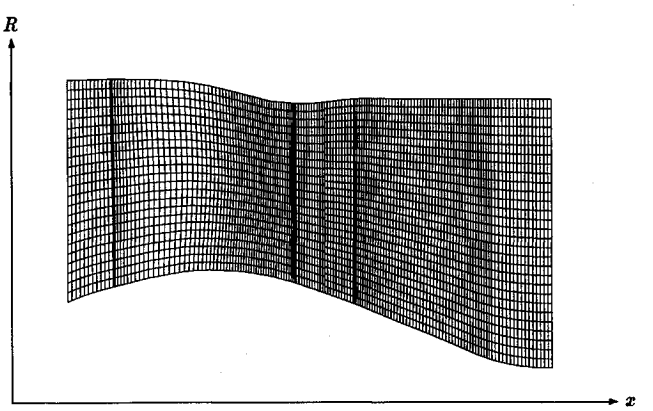

Fig. 1 Side view of a transonic first turbine stage including stator suction and rotor pressure sides.

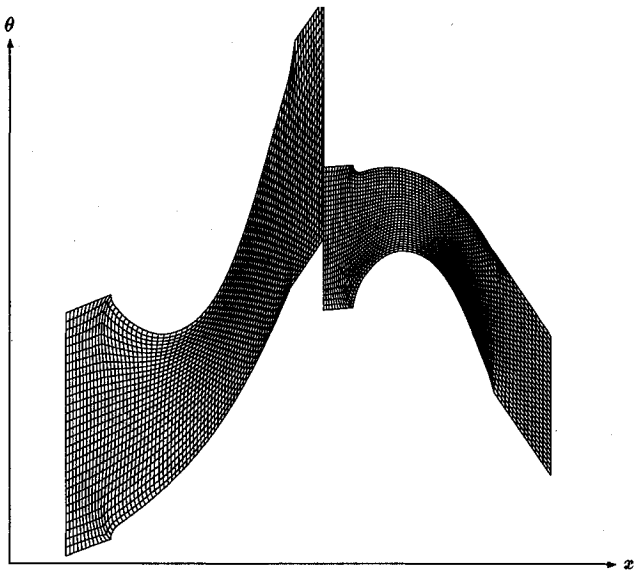

Fig. 2 Mean height blade-to-blade mesh (stator: 80 × 30 × 24, rotor: 77 × 30 × 30 nodes). The stator and the rotor grids shown here are used in the small domain calculations.

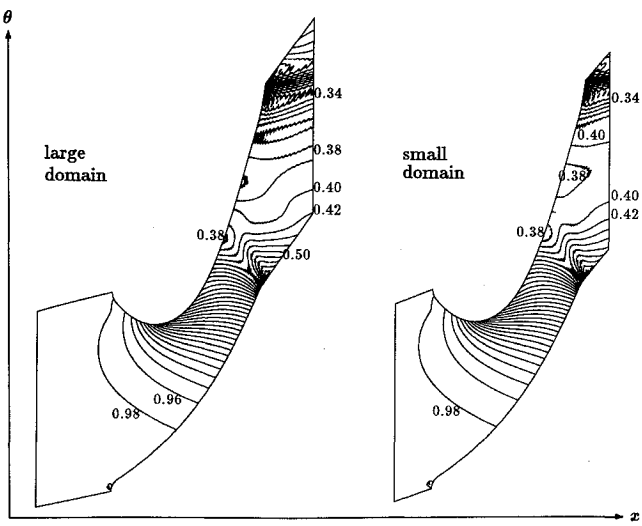

Fig. 3 Stator midspan pressure contours ($p/p_{t\text{inl}}$) using quasi-three-dimensional nonreflecting boundary conditions, $M_{\text{out}} = 1.2$. Isolated stator calculations.

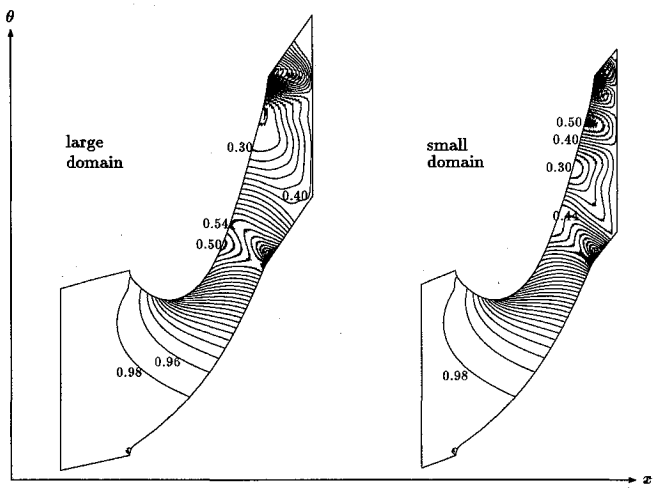

Fig. 4 Stator midspan pressure contours ($p/p_{t\text{inl}}$) using reflecting boundary conditions at the outflow, $M_{\text{out}} = 1.2$. Isolated stator calculations.

boundaries introduces an error which is proportional to the square of the steady-state perturbation at the inflow and the outflow. However, the error is unnoticeable at the inflow and very much smaller at the outflow than the error introduced in the solution by using the standard boundary conditions, which impose uniform exit pressure (see Fig. 4). Using nonreflecting boundary conditions, the local maximum mismatch in pressure between the two solutions of Fig. 3 is less than 4% of the vane exit dynamic head. Clearly, the formulation of the quasi-three-dimensional nonreflecting boundary conditions allows the flow to adjust circumferentially (and also radially as seen later on) to account for the presence of the stator trailing edge. On the other hand, using the standard one-dimensional b.c., the outgoing shocks produce reflected expansion waves which greatly contaminate the solution on the blade (see Fig. 5). These spurious reflections produce a local error in pressure (compared to the solution on the large domain with quasi-three-dimensional b.c.) which is up to 43% of the vane average exit dynamic head. Therefore, the nonreflecting boundary conditions give a major improvement in accuracy.

The midspan blade surface pressure computed by using the quasi-three-dimensional and the one-dimensional formulations on the small and the large domain are compared in Fig. 5, where the inlet stagnation pressure $p_{t\text{inl}}$ is used as a reference. Notice that all disturbances produced by the outlet boundary (in particular the spurious reflections produced by the one-dimensional b.c.) do not propagate ahead of the choked throat, which is consistent with inviscid flow theory. Thus, the four solutions are identical from the inlet to the throat. Due to the strong shock/exit boundary interaction in the one-dimensional formulation, the location of the outlet surface affects the shocks' reflections, i.e., the solutions on the two domains are different with multiple wave reflections on the small one. This local behavior also produces average changes. For instance, the one-dimensional boundary condition formulation leads to a change in the flux-averaged turning angle compared to the quasi-three-dimensional b.c., as seen in Fig. 6. In a stator/rotor interaction this average change in the stator swirl angle can lead to a change in the rotor relative incidence angle of several degrees, and thus significantly affect the rotor loading.

The steady-state results for four coupled transonic stator/rotor calculations are summarized in Figs. 7–9.To achieve an accurate basis for comparison, the small domain results were computed using circumferentially averaged exit pressures $p_r(R)$ obtained from the large domain calculations. Notice that in a full stage computation the matching of the stator and the rotor flow at the interface is done automatically without any user intervention. In these four computations, the quasi-three-dimensional b.c. have been used at the stator inlet and outlet as well as at the rotor inlet. Thus, relative to the calculations using the quasi-three-dimensional formulation at all inlets/

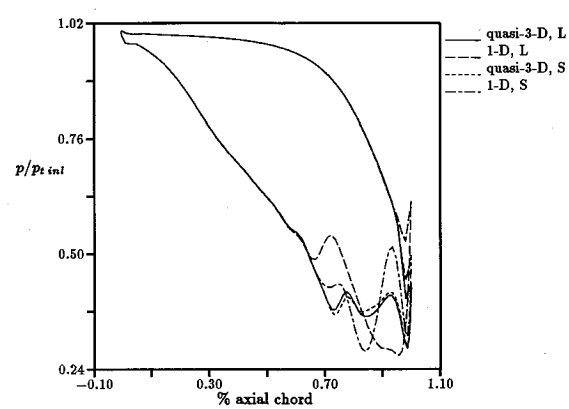

Fig. 5 Midspan stator blade pressure using nonreflecting and reflecting b.c. Isolated stator calculations. L: large domain, S: small domain.

outlets, the introduction of the one-dimensional b.c. at the rotor outlet does not visibly affect the vane flowfield. However, the rotor field is affected through the trailing edge reflected shock which is clearly apparent. It should be pointed out that in the case of a calculation performed with one-dimensional b.c. implemented at the stator inlet, at the interface and at the rotor exit, the discrepancies between the one-dimensional and the three-dimensional formulations would be much larger. As mentioned in the preceding section, the use of one-dimensional b.c. at the stator outlet does affect

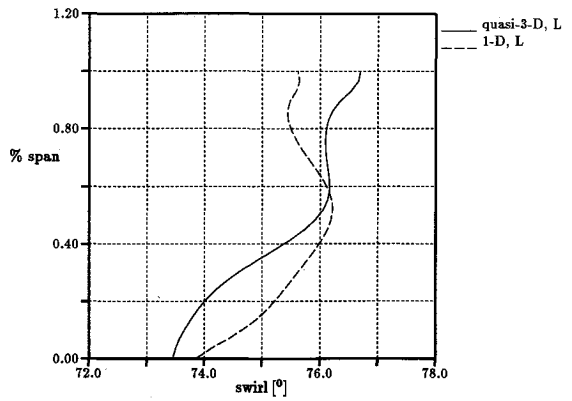

Fig. 6 Flux-averaged turning angle at the large domain stator exit using nonreflecting and reflecting b.c. Isolated stator calculations.

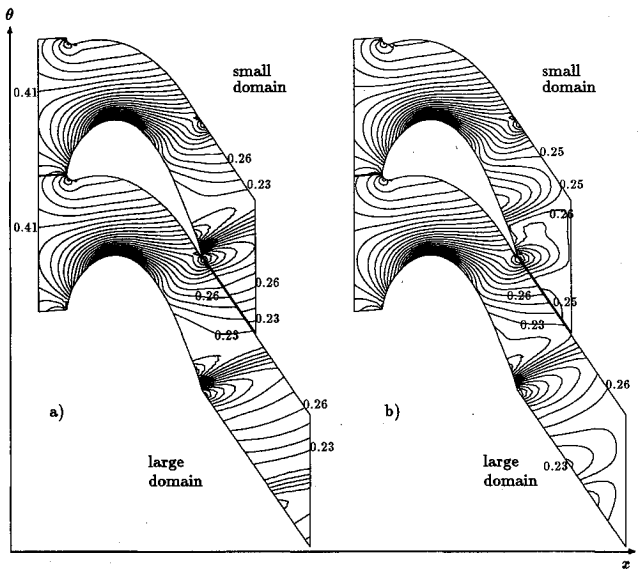

Fig. 7 Rotor midspan pressure contour ($p/p_{t_{inl}}$), M_{out} = 1.1. Coupled stator/rotor calculations: a) quasi-three-dimensional nonreflecting b.c., and b) standard one-dimensional reflecting b.c. at rotor outlet.

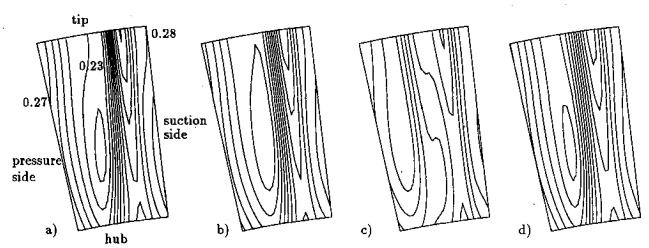

Fig. 8 Rotor blade-to-blade and hub-to-tip pressure contours ($p/p_{t_{inl}}$) at 20% chord downstream of the trailing edge (equals halfway between trailing edge and small domain exit). Coupled stator/rotor calculations. Increments = 0.01: a) quasi-three-dimensional nonreflecting b.c. small domain, b) large domain, c) standard one-dimensional reflecting b.c. (at rotor outlet) small domain, and d) large domain.

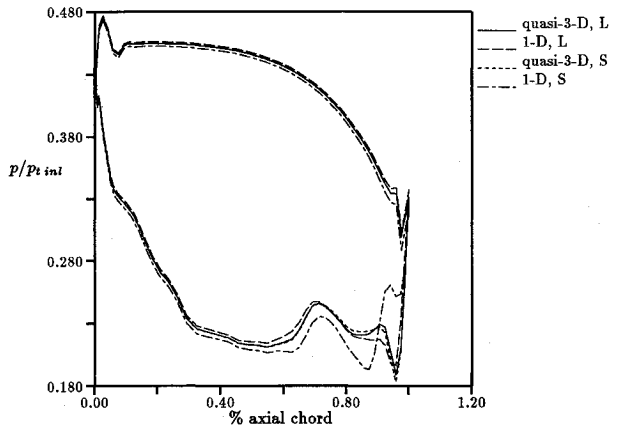

Fig. 9 Midspan rotor blade pressure using nonreflecting and reflecting b.c. Coupled stator/rotor calculations. L: large domain, S: small domain.

the rotor inlet conditions. Thus, the rotor flowfield in turn produces a change in the average stator/rotor interface pressure.

The rotor-relative exit Mach number is very close to unity. It has been numerically observed that while the flow is converging to a steady-state solution, the exit boundary condition "switches" from subsonic to supersonic and vice versa, until the flow at lower radii settles to an average supersonic exit Mach number, whereas the flow closer to the tip is subsonic. This point is important to notice, for the implementation of the nonreflecting boundary conditions requires a Fourier transform in the subsonic case, but none in the supersonic case. No anomalous behavior has been observed during the transient stages of the calculation procedure, and, as seen in Fig. 8, a smooth transition from the supersonic hub flow to the subsonic tip flow occurs in the steady-state solution. Thus, the quasi-three-dimensional formulation performs well at all radii. The pressure plots in Fig. 9 demonstrate that as far as the blade loading is concerned, the use of the quasi three-dimensional formulation gives good results.

The rotor results point out that by extending the computational domain sufficiently far downstream, the results calculated using the one-dimensional formulation tend to match the quasi-three-dimensional b.c. solution (Figs. 7 and 9). This is consistent with both the quasi-three-dimensional and the one-dimensional b.c. formulations since these two techniques give the same results when applied to a uniform flow as it develops here in the constant area duct downstream of the rotor. However, as mentioned earlier this is true only because the rotor exit boundary condition alone is altered from being either quasi-three-dimensional or one-dimensional. (In order to show the effects of imposing the standard one-dimensional b.c. at one particular location, the full stage calculations presented here were computed with only the rotor exit boundary condition formulation modified to be either quasi-three-dimensional nonreflecting or one-dimensional.) Hence, only minor differences in pressure exist (i.e., less than 2% of the vane pressure drop) between the solutions computed with nonreflecting b.c. and the solution using the one-dimensional b.c. formulation on the large domain (Fig. 9). This type of behavior is not apparent in the isolated stator computations of Figs. 3 and 4 partly due to the downstream duct area change and the location of the large domain exit boundary which is still too close to the stator trailing edge. The one-dimensional b.c. formulation applied on the small domain produces errors up to 17% of the vane average pressure drop.

The results for the subsonic flow in a linear turbine cascade are presented in Fig. 10. In this case no radial variations exist and the quasi-three-dimensional formulation reduces to the exact two-dimensional nonreflecting boundary conditions where

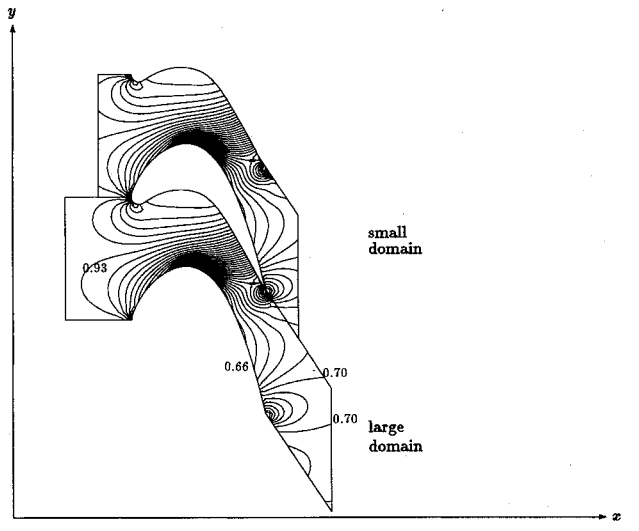

Fig. 10 Pressure contours ($p/p_{t_{inl}}$) using quasi-three-dimensional nonreflecting boundary conditions, $M_{out} = 0.75$. Linear cascade. Increments = 0.01.

only second-order nonlinear errors can arise. However, in this shock-free flow these are very small as shown by the virtual perfect match of the pressure contours between the small and the extended domain calculations (the discrepancy in pressure between the two solutions is smaller than 0.001 times the exit dynamic head).

VII. Conclusions

A theory for the construction of steady-state quasi-three-dimensional nonreflecting boundary conditions has been developed and applied to the Euler equations. The boundary condition formulation is derived using Fourier analysis applied to the linearized equations. A fundamental approximation is that radial effects are accounted for in the average mode only. In the absence of any radial variations, the boundary conditions are exact within the linear theory.

The quasi-three-dimensional formulation has been implemented for transonic and subsonic axial flow turbomachine calculations with realistic operating conditions and for standard designs. In the transonic case where a shock wave crosses the computational boundary, the solution is virtually independent of the position of the computational domain limits with local discrepancies in pressure less than 2% of the vane average pressure drop, which compares to 24% when using the standard one-dimensional formulation. Hence, the second-order nonlinear errors together with the error due to the uncoupling of the radial and tangential variations are very much smaller than the ones introduced in the solution when using the standard one-dimensional approach. In the subsonic case the solution is completely independent of the position of the far-field boundaries.

Acknowledgments

This work has been performed under a research grant from Rolls-Royce PLC, supervised by P. Stow.

References

[1]Kreiss, H.-O., "Initial Boundary Value Problems for Hyperbolic Systems," *Communications of Pure and Applied Mathematics*, Vol. 23, 1970, pp. 277–298.

[2]Engquist, B., and Majda, A., "Absorbing Boundary Conditions for the Numerical Simulation of Waves," *Mathematics of Computation*, Vol. 31, July 1977, pp. 629–651.

[3]Ferm, L., "Open Boundary Conditions for External Flow Problems," Computing Science Rept. 108, Uppsala Univ., Uppsala, Sweden, Feb. 1987.

[4]Ferm, L., and Gustafsson, B., "A Down-Stream Boundary Procedure for the Euler Equations," *Computer and Fluids*, Vol. 10, No. 4, 1982, pp. 261–276.

[5]Hirsch, C., and Verhoff, A., "Far-Field Numerical Boundary Conditions for Internal and Cascade Flow Computations," AIAA Paper 89-1943-CP, 1989.

[6]Giles, M. B., "Non-Reflecting Boundary Conditions for Euler Equation Calculations," *AIAA Journal*, Vol. 28, No. 12, 1990, pp. 2050–2058.

[7]Bayliss, A., and Turkel, E., "Far-Field Boundary Conditions for Compressible Flows," *Journal of Computational Physics*, Vol. 48, 1982, pp. 182–199.

[8]Yee, H. C., Beam, R. M., and Warming, R., "Stable Boundary Approximations for the One-Dimensional Inviscid Equations of Gas Dynamics," AIAA Paper 81-1009, 1981.

[9]Giles, M. B., "Non-Reflecting Boundary Conditions for the Euler Equations," Massachusetts Inst. of Technology Computational Fluid Dynamics Lab. Rept. TR-88-1, 1988.

[10]Whitham, G. B., *Linear and Nonlinear Waves*, Wiley, New York, 1988.

[11]Ni, R.-H., "A Multiple Grid Scheme for Solving the Euler Equations," *AIAA Journal*, Vol. 20, No. 11, 1981, pp. 1565–1571.

[12]Saxer, A. P., and Giles, M. B., "Inlet Radial Temperature Redistribution in a Transonic Turbine Stage," AIAA Paper 90-1543, 1990.

[13]Saxer, A. P., "A Numerical Analysis of 3-D Inviscid Stator/Rotor Interactions Using Non-Reflecting Boundary Conditions," Ph.D. Dissertation, Massachusetts Inst. of Technology, Cambridge, MA, June 1992; see also Massachusetts Inst. of Technology Gas Turbine Lab. Rept. 209.